# On the phase velocity in between weak and strong plasma edge turbulence

**P Manz**[1] , **D Prisiazhniuk**[1] , **T Happel**[1]**, S Freethy**[1]**, K Hallatschek**[1]**,
B D Scott**[1]**, U Stroth**[1,2] **and the ASDEX Upgrade Team**

[1] Max-Planck-Institut für Plasmaphysik, Boltzmannstr.2 ,85748 Garching, Germany
[2] Physik-Department E28, Technische Universität München, James-Franck-Str. 1, 85748 Garching, Germany

E-mail: peter.manz@ipp.mpg.de

CrossMark

## Abstract

The influence of strong fluctuation levels on the phase velocity is studied just inside the last closed flux surface in the edge of magnetized confined plasmas by means of gyrofluid simulations. Linear features as growth rates and dispersion can be suppressed by small-scale vorticity generated by nonlinear self-sustainment. Measurements of the phase velocity by different diagnostic techniques could still provide finite values, which are not a result of linear instabilities, but are due to the nonlinear redistribution of spectral energy.

Keywords: weak turbulence, strong turbulence, phase velocity, drift wave, self-sustainment, plasma edge

(Some figures may appear in colour only in the online journal)

## 1. Introduction

The edge of magnetized confined plasmas is characterized by steep gradients and is subject to a large number of different modes resulting from various linear instabilities and diverse nonlinear self-organized phenomena. It is widely thought that an underlying instability grows and excites the turbulence by nonlinear saturation [1]. During such a process various features of the underlying instability may be transmitted to the turbulence [2–4]. In plasma turbulence it is also common to classify the turbulence according to its driving instability; the turbulence is not universal, and is called, for example, ion temperature gradient (ITG) or trapped electron mode turbulence. Different modes or instabilities can be distinguished by their size, cross-phase relations between different quantities (as density, potential, electron and ion temperature, and heat fluctuations), and their dispersion relation between wavenumber $k$ and frequency $\omega$. An overview of the propagation direction, cross-phases, and typical sizes of the most relevant instabilities for the plasma edge can be found in [5].

Since cross-phase relations are commonly not available in experiments, the phase velocity is usually one of the key identifiers of underlying instability. This may be a proper treatment at the low fluctuation level typically observed in the plasma core.

In ideal fluid turbulence the nonlinearity is usually strong enough that linear instabilities are to a large extent negligible. Here, turbulence is considered to be universal and not classified according to its initial instability. Furthermore, at some fluctuation level the plasma turbulence should become universal. In the present contribution we study how plasma turbulence can suppress linear features as growth rates and eigenfrequencies. Plasma turbulence inside the edge of the confined plasma is investigated in the low-confinement regime. This region is characterized by high fluctuation levels. In the region just inside the confined region, the turbulence exhibits close to Gaussian statistics, and is to a high degree self-similar and non-intermittent. In ASDEX Upgrade, Joint European Torus (JET), and Alcator C-Mod, just inside the separatrix the distribution function is close to Gaussian [6–8], as in simulations similar to those presented in [9]. In the scrape-off layer, just outside the separatrix, filamentary transport becomes important [10, 11]. These filaments exhibit characteristic sizes [12], and turbulence in the scrape-off layer is not self-similar, but intermittent [13].
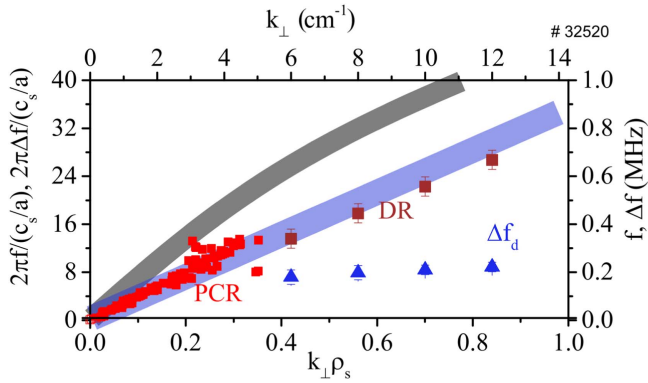
**Figure 1.** Frequency versus wavenumber measured by DR (dark red squares □) and PCR (red squares □) at the plasma edge ($\rho_{\text{pol}} = 0.985$) of a typical ASDEX Upgrade L-mode plasma at a temperature of $T_{\text{e}} = 124$ eV. The frequency is normalized to the cold ion sound speed $c_{\text{s}}$, and the wavenumber to $\rho_{\text{s}} = 0.7$ mm calculated with the magnetic field on axis $B = 2.6$ T. The frequency broadening $\Delta f$ (blue triangles △) is about one-third of the measured frequency. The corresponding perpendicular velocity $\partial f / \partial k$ is not varying with the wavenumber within the error bars. The estimate for the $E \times B$ velocity is indicated by the blue shaded area, and an estimate of the drift wave dispersion relation is indicated by the black shaded area.

In the following, experimental observations of the phase velocity inside the edge of the confined region are summarized (section 1.1). Particular attention is paid to experiments at ASDEX Upgrade. Different measurement techniques to determine the phase velocity are discussed in section 1.2. The concepts of weak and strong turbulence regimes are introduced in section 1.3. With the help of simulations (details given in section 2) the influence of the strength of broadband turbulence on the measurements of a phase velocity are investigated. These are studied in a simulated case of weak turbulence (section 3) and strong turbulence (section 5), and in a regime between weak and strong turbulence corresponding to the experimental situation at ASDEX Upgrade (section 4). It will be shown that the high fluctuation level of the turbulence (in particular the high level of vorticity fluctuations) in the plasma edge is strong enough to suppress linear features of the plasma turbulence. Measured finite phase velocities can be a result of the turbulent cascade independent of an underlying instability. A summary and conclusions are given in section 6.

## 1.1. Measurements of the phase velocity

Measurements in ASDEX Upgrade with Doppler reflectometry (DR) show no significant phase velocity in the plasma edge, and the measured velocity is approximately the $E \times B$ background velocity [14], showing no signs of dispersion [15]. This has been also observed in W7-AS [16], and seems to be in contradiction to drift waves being the dominant instability in the plasma edge from a linear perspective. On the other hand, finite phase velocities have been reported from the plasma core in ASDEX Upgrade [17, 18] and from the plasma at around $r/a = 0.8$ in Tore Supra [19].

For the purpose of illustration, an example of measurements at different wavenumbers is shown in figure 1. The data is shown in normalized dimensionless units (left and bottom axis)

and in dimension-assigned units (right and top axis). Measurements have been done at the plasma edge in the confinement region ($\rho_{\text{pol}} = 0.98$) which is expected to be drift wave-dominated [20]. The dispersion relation of drift waves is given by

$$\omega_l = \frac{u_{\text{e,dia}} k_y}{1 + (\rho_{\text{s}} k_\perp)^2}. \tag{1}$$

The index $l$ in the frequency $\omega_l$ distinguishes the linear frequency from the nonlinear frequency. Drift waves exhibit a phase velocity $\omega_l / k$ close to the electron diamagnetic velocity $u_{\text{e, dia}}$, and propagate binormal ($k = \mathbf{k}_y$) to the magnetic field and radial direction ($\mathbf{k}_x$). The perpendicular plane is spanned by the radial and binormal directions ($\mathbf{k}_\perp = \mathbf{k}_y + \mathbf{k}_x$). Due to polarization effects, the phase velocity is reduced by $(\rho_{\text{s}} k_\perp)^2$ at structures close to the drift-scale $\rho_s = \sqrt{T_e m_{\text{i}}} / (eB)$, with elementary charge $e$, magnetic field strength $B$, ion mass $m_{\text{i}}$, and electron temperature $T_{\text{e}}$. DR with a movable mirror allows one to probe varying wavenumbers ($6 < k_\perp < 12$ cm$^{-1}$) during the discharge, and the poloidal correlation reflectometer (PCR) [15] is sensitive at low wavenumbers ($k_\perp < 3$ cm$^{-1}$). The measured Doppler frequency shows a linear relationship to the probed wavenumber. The measured frequencies by the PCR aligns well with those measured by the DR. The radial electric field in the plasma edge is given in first-order by its ion diamagnetic contribution with possible additional contributions from the neoclassical viscosity and from the Reynolds stress [21]. In ASDEX Upgrade H-modes plasmas, the radial electric field is approximately its ion diamagnetic contribution [22]. In L-mode, the collisionality can be expected to be higher, and therefore neoclassical effects can be expected to be less important. In the I-phase [23], where zonal flows are thought to be important [24, 25], the radial electric field in ASDEX Upgrade also follows its ion diamagnetic contribution [26]. Therefore, it seems plausible to assume that the radial electric field and $E \times B$ flow can also be approximated by their diamagnetic contributions in L-mode in ASDEX Upgrade. The $E \times B$ velocity has been estimated by $u_{E \times B} \approx (1/en) \nabla p_i \approx (1/en) \nabla p_e$ to be around 4 km s$^{-1}$ (indicated by the blue shaded area in figure 1), where the measured dispersion in the phase velocity is small ($< 0.35$ km s$^{-1}$) and is within the error bars of the measurements. A possible phase velocity is significantly below the electron diamagnetic velocity, which is of the order of $u_{E \times B}$, as indicated by the black shaded line in figure 1.

## 1.2. Measured dispersion dependent on the measurement technique

To infer spatial characteristics from temporal signals experimentally, one must map time to space; this is mainly motivated by Taylor's hypothesis of frozen turbulence [27]. It is assumed that at a point the change of turbulent velocity fluctuations in time can be directly related to their spatial change via the mean convection velocity. In the fifties it was shown that the hypothesis breaks down and is restricted to a limited range of wavenumbers (or frequencies) for shear flows [28]. The applicability of Taylor's hypothesis also depends on the fluctuation level: to be valid, turbulent velocity fluctuations must be significant smaller than the mean velocity [28].

Due to the power distribution in the wavenumber–frequency plane $P(k, \omega)$, the power of a single frequency will have contributions from multiple wavenumbers. This results in two different ways to determine average wave velocities given by the direction of integration. One can integrate in the wavenumber direction, keeping frequency constant, or integrate in the frequency direction while keeping the wavenumber constant. Depending on the shape and broadening of the wavenumber–frequency distribution, different answers will be obtained, as we will see in the following.

For example, by choosing the wavenumber to be constant, $k_0$, we take a cut in the frequency direction. The average frequency is defined by

$$\langle \omega \rangle (k_0) = \frac{\int P(k_0, \omega) \omega \mathrm{d}\omega}{\int P(k_0, \omega) \mathrm{d}\omega}. \tag{2}$$

DR measures a power spectrum $P(k_0, \omega)$ at a given wavenumber $k_0$, from which a wavenumber-dependent phase velocity $u(k_0) = \frac{\langle \omega \rangle (k_0)}{k_0}$ can be estimated in principle. Since the low-frequency range is often corrupted by the directly reflected microwave beam, this analysis approach is often misleading, and the Doppler shift should be determined by fitting a Gaussian to the power spectrum.

By choosing a constant frequency $\omega_0$ to examine wave velocities, cuts along the wavenumber direction in $P(k, \omega_0)$ give an average wavenumber defined by

$$\langle k \rangle (\omega_0) = \frac{\int P(k, \omega_0) k \mathrm{d}k}{\int P(k, \omega_0) \mathrm{d}k}. \tag{3}$$

A wave velocity can be estimated by $u(\omega_0) = \frac{\omega_0}{\langle k \rangle}$. Measuring a wavenumber by estimating it by the phase difference of spatially separated points leads to such estimates. If fluctuations can be represented by an eikonal $\sim \exp(i\theta)$ with $\theta = kx - \omega t$, the effective or pseudo wavenumber [29] is given by $\langle k \rangle (\omega) = \frac{\partial \theta}{\partial x}$. Mode numbers of magnetic signals are usually estimated in this way [30]. Time delay estimation (TDE) works in a similar manner. Here, the phase is measured at two spatially displaced positions $\theta(x, t)$ and $\theta(x + \Delta x, t)$. The time lag $\Delta t$ is estimated, where both signals are in phase. Hence, $\theta(x, t) = \theta(x + \Delta x, t + \Delta t)$ or $k\Delta x = \omega \Delta t$. From this, a frequency-dependent phase velocity can be directly inferred $u_{ph}(\omega) = \frac{\omega}{k} = \frac{\Delta x}{\Delta t}$. The spatial displacement $\Delta x$, a time delay $\Delta t$, and the frequency at which the time delay is measured are determined. What is actually estimated here is an effective phase velocity $\langle u \rangle_{\mathrm{TDE}}(\omega) = \frac{\omega}{\langle k \rangle_{\mathrm{TDE}}}$, which corresponds to the effective wavenumber $\langle k \rangle_{\mathrm{TDE}}(\omega) = \frac{\omega}{\Delta x} \Delta t$.

There are additional problems, like propagation into the radial direction or eddy tilting, that can be diminished by taking into account multiple spatial points; TDE methods that include multiple spatial points [31–33] or velocimetry [34] also rely basically on the same assumptions. However, if the measured field contains all important spatial scales of motion, it should be, in principle, appropriate to recover the phase velocity. Nearly all measurements of velocities done with Langmuir probe arrays, gas-puff or electron cyclotron

emission imaging, beam emission spectroscopy, correlation reflectometry, or phase-contrast imaging measure an effective wavenumber $\langle k \rangle (\omega)$.

In this study, these two different measurement methods for the estimation of phase velocities are investigated in the case between weak and strong plasma edge turbulence.

### 1.3. Turbulence regimes

The distinction between weak and strong turbulence goes back to Kadomtsev [1]; the latest review can be found in [35]. The regimes of turbulence are distinguished by the strength of fluctuations represented by spectral broadening. The frequency broadening is defined by

$$\Delta \omega (k) = \sqrt{\frac{\int P(k, \omega) \omega^2 \mathrm{d}\omega}{\int P(k, \omega) \mathrm{d}\omega} - \langle \omega \rangle^2}. \tag{4}$$

The wavenumber broadening is defined by

$$\Delta k (\omega) = \sqrt{\frac{\int P(k, \omega) k^2 \mathrm{d}k}{\int P(k, \omega) \mathrm{d}k} - \langle k \rangle^2}. \tag{5}$$

In weak turbulence, a wave-like instability grows, and its nonlinear saturation is responsible for the turbulence. To retain its wave-like features, the frequency is similar to the linear eigenfrequency $\langle \omega \rangle \sim \omega_l$, and the growth rate is smaller than the linear eigenfrequency $\gamma_l \ll \omega_l$. The weak turbulence regime is also called wave turbulence. The growth rate of the instability is balanced by nonlinear saturation $\gamma_l \sim \Delta \omega$. Weak turbulence is characterized by small frequency broadening $\Delta \omega \ll \omega_l$.

In the strong turbulence regime the nonlinearities dominate, and the turbulence is independent of the excitation process. Strong turbulence is characterized by strong frequency broadening $\Delta \omega$ exceeding the analytically expected eigenfrequency $\Delta \omega \gg \omega_l$. As a result, strong turbulence does not feature a linear wave frequency due to the short decorrelation time $\tau \approx 1/\Delta \omega$ resulting in $\gamma_l \ll \Delta \omega$, $\omega_l \ll \Delta \omega$. Equivalent considerations are valid for the wavenumber.

That the nonlinearity is not dominant in the weak turbulence case does not mean that it does not lead to a redistribution of spectral energy and that cascades are not present. It just means that the turbulent spectral power $P(k, \omega)$ is tightly bound to the linear dispersion relation in the wavenumber–frequency plane, as indicated by the gray region in figure 2(a). The spectral power can be redistributed along the dispersion relation, and a cascade can be observed as indicated by the blue upper spectrum in figure 2(a). However, vertical and horizontal cuts through the wavenumber–frequency plane, corresponding to frequency (wavenumber) spectra at a given wavenumber (frequency), show no cascades and just the dispersion. In the case of strong turbulence (figure 2(b)), the dispersion relation can be neglected, and the spectral power mainly follows the Doppler shift of the background flow. Due to the strong nonlinearity, the spectral power spreads in all directions with the tendency to lower frequencies and wavenumbers in the two-dimensional case.
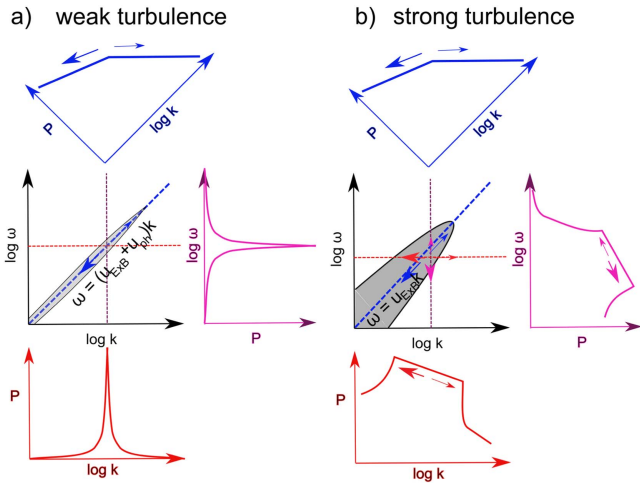
**Figure 2.** Artist's view of spectral features of weak and strong turbulence.

These can also be observed in the frequency (wavenumber) spectra at a given wavenumber (frequency).

## 2. Simulation set up

Simulations for a circular plasma cross-section with toroidal axisymmetry have been carried out with the three-dimensional gyrofluid electromagnetic turbulence model GEMR [36, 37]. GEMR simulates the densities, parallel velocities, parallel and perpendicular temperatures, and parallel and perpendicular parallel heat fluxes for ions and electrons, respectively. The coordinate system is aligned with the equilibrium magnetic field. Despite being a $\delta$-f limited code, the gradients evolve freely, and GEMR is a global model. Details on the self-consistent treatment of the profiles and magnetohydrodynamic (MHD) equilibrium can be found in [36]. The main input parameters of GEMR are a smallness parameter $\delta = \rho_s/a$, a normalized plasma beta $\beta$, and a normalized collisionality $\nu = a\nu_e/c_s$, with $\nu_e$ being the inverse Braginskii electron collision time. Simulations are carried out at ASDEX Upgrade ($R = 1.65$ m, $a = 0.5$ m, $B = 2.4$ T, $q_s = 4.6$). The coordinate system ($x$, $y$, $s$) is in the radial, binormal, and parallel direction to the magnetic field. The simulations are performed on a $128 \times 512 \times 16$ grid, where only the drift plane ($128 \times 512$) at the outboard midplane is analyzed here. The simulations cover the region $0.96 < \rho < 1.04$.

About 1 ms is simulated. The time series is split up into six subwindows. The frequency resolution is about $a/c_s$. For each subwindow the wavenumber–frequency power spectrum of the density fluctuations $\tilde{n}(y, t)$ at a given flux surface $x = \rho$ at the outboard midplane $s = 0$ has been calculated by the two-dimensional Fourier transform $\tilde{n}(y, t) \rightarrow \tilde{n}(k, \omega)$. All points in the binormal direction have been used for the spatial Fourier transform. The presented wavenumber–frequency power spectra $P(k, \omega) = \langle \tilde{n}(k, \omega)\tilde{n}^*(k, \omega) \rangle$ shown in the following are averaged $\langle \cdot \rangle$ over these subwindows. Since the spectra are shown at one particular flux surface, effects due to a finite radial measurement volume, which are present for
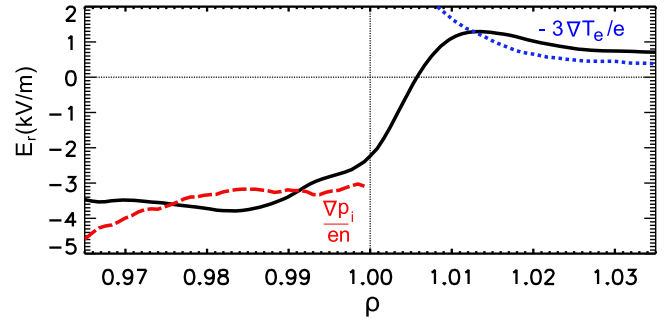


**Figure 3.** Strong turbulence case: radial electric field (black solid line), ion pressure contribution (red dashed line), and sheath potential contribution (blue dotted line) to the radial electric field.

every real diagnostic, are not taken into account. Furthermore, the spectra shown in the following are in a region with a moderate amount of shearing. Therefore, structures propagating in opposite directions, as often observed in experiments [38–41], are not observed here.

Typical experimental parameters at the last closed flux surface as the reference flux surface are chosen. The case corresponding to the experimental situation (section 4) is at $n_e = 2 \cdot 10^{19}$ m$^{-3}$, and $T_e = T_i = 120$ eV, corresponding to $\delta = 1.32 \cdot 10^{-3}$, $\beta = 8.39 \cdot 10^{-5}$, and $\nu = 4.08$. The gradient scale lengths are fixed and not allowed to evolve, and are chosen to be $L_n = 0.5L_{Te} = 0.5L_{Ti} = 2.5$ cm in the experimental situation. The strong turbulence case (section 5) is at $n_e = 2 \cdot 10^{19}$ m$^{-3}$, and $T_e = T_i = 100$ eV, corresponding to $\delta = 1.20 \cdot 10^{-3}$, $\beta = 6.99 \cdot 10^{-5}$, and $\nu = 5.88$. Initial gradient scale lengths are chosen to be $L_n = 0.5L_{Te} = 0.5L_{Ti}$. The radial resolution is 0.65 $\rho_s$, and the resolution of the binormal plane is 0.55 $\rho_s$. We expect drift wave turbulence under these conditions [20].

The gradients evolve in the strong turbulence case (section 5). During the initial phase the density gradient relaxes, and the ITG effectively steepens compared to the density gradient $L_n = (2/3)L_{Ti} = 5$ cm. The radial electric field is shown in figure 3; it is dominated by its ion pressure contribution in the confined region and by the sheath potential in the scrape-off layer. The turbulence shows different features depending on the wavenumber. At low wavenumbers ($k\rho_s < 0.2$), the strong potential perturbations correspond to resistive ballooning modes (see figure 4). At higher wavenumbers ($k\rho_s > 0.2$), density and potential fluctuation amplitudes are similar, which is characteristic of drift wave turbulence. At even higher wavenumbers ($k\rho_s > 0.6$), the ion temperature fluctuations are strongest, pointing to ITG drift wave turbulence.

For the sake of completeness, a weak turbulence case is presented in section 3. Weak turbulence can be obtained for small gradients appearing, for example, in the core. The reference surface is chosen to be at $\rho = 0.5$ with $n_e = 4.5 \cdot 10^{19}$ m$^{-3}$, and $T_e = T_i = 2$ keV. The simulations cover the region $0.3 < \rho < 0.7$, with gradient scale lengths of $L_{Ti} = L_{Te} = 0.3L_n = 20$ cm. ITG turbulence can be expected in such a case. The corresponding GEMR input
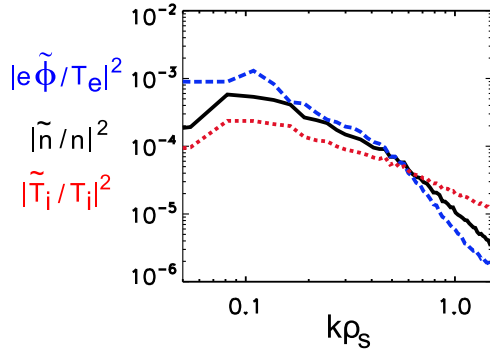
**Figure 4.** Strong turbulence case: Wavenumber spectra of normalized potential (blue), density (black), and ion temperature (red) fluctuations. Potential perturbations are strongest at low wavenumbers, corresponding to ballooning modes; at higher wavenumbers, density and potential fluctuations are similar, and the ion temperature fluctuations are strongest, pointing to ITG drift wave turbulence.

parameters are $\delta = 5.38 \cdot 10^{-3}$, $\beta = 3.15 \cdot 10^{-3}$, and $\nu = 0.03$. The results are shown in section 3.

## 3. Weak turbulence case $\Delta\omega < \omega_l$

The wavenumber–frequency power spectrum $P(k, \omega)$ of density fluctuations in the plasma frame of reference at $\rho = 0.5$ are shown in figure 5(a) in the late growth phase of the simulation. The directions are defined positive for the ion diamagnetic direction, and negative in the electron diamagnetic direction. Since $\omega/k$ is positive, a clear phase velocity in the ion diamagnetic direction can be observed, which is a sign of ITG turbulence. The linear phase velocity can be measured from equation (2), and is shown by the black line in figure 5(c). Most of the turbulence activity is restricted to this very narrow line. This situation corresponds to the weak turbulence case, but it is not saturated yet. The turbulence saturates at a fluctuation level of about $\tilde{n}/n \approx 1$ %. In the saturated phase the turbulence becomes more broadband, as shown by figure 5(b). The averaged frequency $\langle\omega\rangle$, as shown by the red dotted line in figure 5(c), is reduced compared to the growth phase, but a phase velocity in the ion diamagnetic direction is clearly observed. The average frequency $\langle\omega\rangle$ is above the frequency broadening $\langle\omega\rangle > \Delta\omega$ (shown by the blue line in figure 5(c)). Therefore, this case is in the weak turbulence regime even though it is not ideal because the frequency does not exceed the broadening much. With respect to the linear frequency (shown by the black line in figure 5(c)), the turbulence is in the weak turbulence regime. The underlying instability (ITG) can imprint its linear phase velocity to the turbulence. The linear frequency significantly exceeds the frequency broadening $\omega_l \sim \langle\omega\rangle \gg \Delta\omega$ and rms vorticity (this will be important later, and is indicated by the gray region in figure 5(c)).

## 4. Experimental parameter case $\Delta\omega \gtrsim \omega_l$

In the typical experimental situation in ASDEX Upgrade presented above, a significant frequency broadening is present;
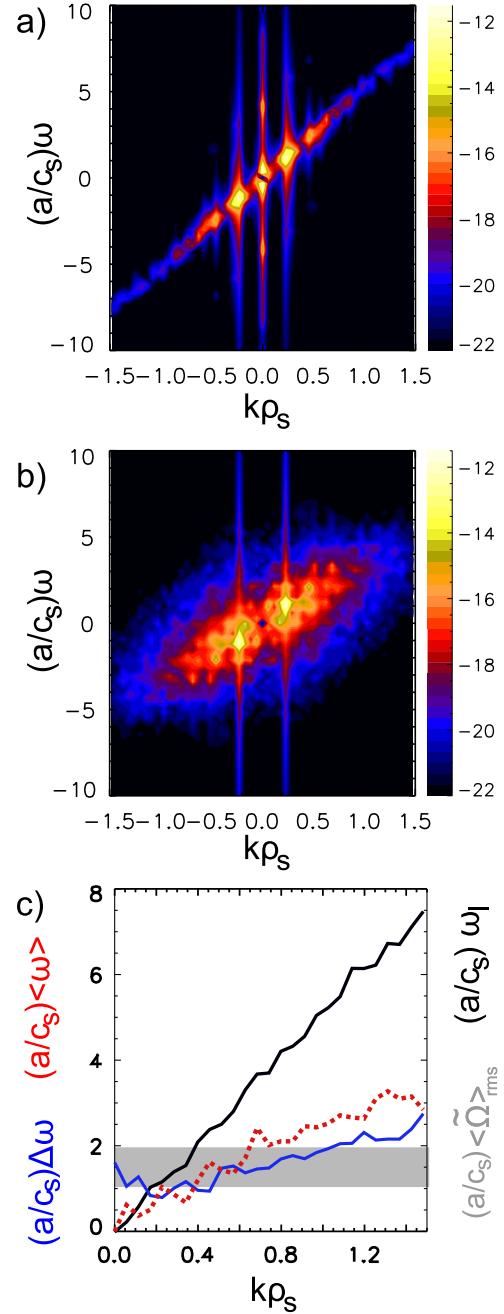


**Figure 5.** Weak turbulence case: wavenumber–frequency power spectrum $P(k, \omega)$ of density fluctuations at $\rho = 0.5$ in the plasma frame in (a) the late growth phase and (b) the saturated phase. (c) Frequency broadening shown by the blue solid line compared to the average frequency in the plasma frame is shown by the black solid (red dotted line) in the growth (saturated) phase. The rms vorticity level is indicated by the gray area. The linear eigenfrequency (black line) exceeds both the frequency broadening and rms vorticity level.

however, it does not exceed the average frequency. In figure 1 the frequency broadening as estimated from DR is $\Delta f_{meas}/\langle f_{meas}\rangle \approx 0.3$. Therefore, typical L-mode plasmas at the plasma edge in ASDEX Upgrade are closer to a weak turbulence regime. Due to the turbulence, the frequency is broadened by $\Delta\omega(k) = k\Delta u + u_{E \times B}\Delta k + \Delta k\Delta u$, where $\Delta k$ is the nonlinear wavenumber broadening and $\Delta u$ is the nonlinear velocity broadening or the velocity spectrum. The measured frequency broadening is
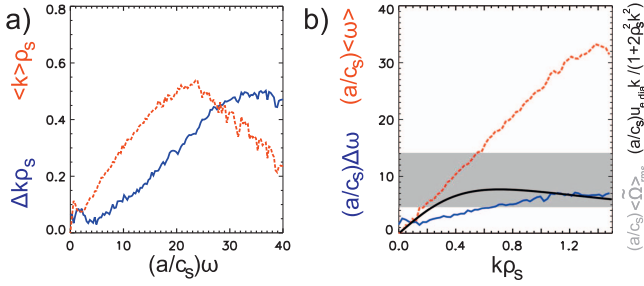
**Figure 6.** Experimental parameter case: (a) wavenumber and (b) frequency broadening shown by blue solid lines compared to the average wavenumber and frequency shown by red dashed lines. The drift wave eigenfrequency is included as a black line, and the rms vorticity level is indicated by the gray area. Data is shown in the laboratory frame of reference. Data is shown from $\rho = 0.980$.



**Figure 7.** Experimental parameter case. (a) Wavenumber–frequency power spectrum $P(k, \omega)$ of density fluctuations at $\rho = 0.980$. The mode at $k\rho_s = 0.1$ is an interchange mode. (b) Average frequency $\langle\omega\rangle(k)$ (red dashed line), the mean $E \times B$ velocity $\omega = u_{E \times B}k$ (blue solid line), phase velocity determined by average wavenumber $\omega/\langle k\rangle$ (red dotted line), fitted mean of the Gaussian in dependence of wavenumber (black dashed line), and corresponding phase velocity determined by TDE (black dotted line). Data is shown in the laboratory frame of reference.

not only due to fluctuations at the probing wavenumber $k_0$, but is also due to the finite spectral resolution $\Delta k_0$ probed [39, 42], resulting in a frequency broadening $2\pi\Delta f_{\text{diag}} = \Delta k_0 \cdot u$. Taking $\Delta k_0 = 2.2$ cm$^{-1}$, we get $\Delta f_{\text{diag}}/\Delta f_{\text{meas}} \approx 0.5$. Since $\Delta f_{\text{diag}}$ gives basically the sensitivity of the diagnostics, it is likely that $\Delta f_{\text{meas}}$ provides the correct estimate of the frequency broadening by the turbulence. At the very least, it is not higher $\Delta\omega < 2\pi\Delta f_{\text{meas}}$. In a conservative approach, the minimum frequency broadening by the turbulence would be $\Delta\omega > 2\pi(\Delta f_{\text{meas}} - \Delta f_{\text{diag}})$, and therefore $\Delta\omega/\langle\omega\rangle \approx 0.15$–0.3.

In contrast to plasma core parameters, a weak turbulence regime in the plasma edge seems to not be easily accessible in GEMR. By fixing the background profiles to the initial conditions, a reduction in the spectral broadening can be obtained. Besides, at very low frequencies the average frequency strongly exceeds the frequency broadening $\langle\omega\rangle(k) \gg \Delta\omega(k)$ (figure 6(b)) by $\langle\omega\rangle(k)/\Delta\omega(k) \approx 4$–7. This is of a similar order as in the experimental observation (figure 1) where the average frequency exceeds the frequency broadening by $\langle\omega\rangle(k)/\Delta\omega(k) \approx 1.5$–3.5 (taking into account broadening by diagnostic effects discussed above, this factor may be assumed to be $\langle\omega\rangle(k)/\Delta\omega(k) \approx 3$–7). An interchange instability is present at these low frequencies. The wavenumber-frequency power spectrum is shown in figure 7(a). The spectral power aligns well with the background $E \times B$ velocity shown by the white line. As seen in figure 7(b), $\langle\omega\rangle(k) \approx u_{E \times B}k$, and no significant wavenumber shift is observed. Approximating velocities by the center of gravity of the frequency [43] using equation (2) is not the usual evaluation method. Commonly, a Gaussian is fitted to the logarithmic power spectrum $P(k_0, \omega)$. The center of the Gaussian is equated with the Doppler shift as the advection velocity. Thus, the background velocity is recovered. The average wavenumber $\langle k\rangle(\omega)$ strongly exceeds the wavenumber broadening $\Delta k(\omega)$ up to roughly $(a/c_s)\omega < 20$ (figure 6(a)). For low frequencies with low frequency broadening $((a/c_s)\omega < 20)$, the phase velocity follows the background velocity only by $\omega/\langle k\rangle \approx u_{E \times B}k$ (figure 7(b)). At higher frequencies with significant broadening in wavenumber space (Figure 6(a)), a propagation in electron diamagnetic direction is observed (figure 7(b)). However, this shift is mainly due to the presence of an interchange mode at
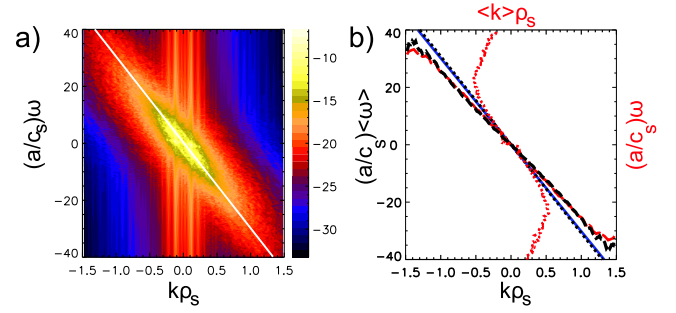
$k\rho_s \approx 0.1$ (figure 7(a)). Also note that the measurements in ASDEX Upgrade do not cover this region. Moreover, a frequency-dependent diagnostic will usually not evaluate equation (3), but instead estimate the velocity by correlation. Indeed, the velocity estimated with TDE using a spatial separation of about 5 mm (black dotted line in figure 7(b)) recovers the background velocity (blue solid line in figure 7(b)), as shown by the overlap of the lines in figure 7(b). In summary, this simulation does not show any significant phase velocity in the plasma frame, nor any dispersion.

How linear features can get lost in drift wave turbulence can be found in [44], which is shortly summarized here. In the weak turbulence case, the linear growth rate balances the nonlinear broadening $\gamma_l \sim \Delta\omega$. This is not the case for fully developed drift wave turbulence in the plasma edge; the linear growth rate is much smaller than the rms vorticity $\gamma_l \ll \langle\tilde{\Omega}\rangle_{\text{rms}}$ [44]. Since the nonlinear spectral transfer is done mainly by the vorticity equation, the rms vorticity should be of the order of the frequency broadening $\langle\tilde{\Omega}\rangle_{\text{rms}} \sim \Delta\omega$. Regarding $\gamma \sim \Delta\omega$, fully developed drift wave turbulence is not in the weak turbulence regime [44].

The transition to turbulence occurs at the beginning of the simulation, and the growth phase can be studied. For $t < 30$ $c_s/a$ the turbulence grows exponentially, as seen by the amplitude in figure 8(a). Due to adiabatic coupling, density fluctuation also induces vorticity fluctuations (figure 8(b)), which also grow exponentially at the beginning of the simulation. The growth rate is about $\gamma_l \approx 0.2$ $c_s/a$, and is carried mainly by an interchange mode at $k\rho_s \approx 0.1$. As the density fluctuation level increases, so does the rms vorticity level. The vorticity is calculated by $\tilde{\Omega} = \nabla_\perp^2(\tilde{\phi} + \tilde{p}_i)$ and takes into account the electrostatic potential and ion pressure fluctuations. At $t \approx 25$ $c_s/a$ the rms vorticity exceeds the linear growth rate. Shortly after this, at $t \approx 35$ $c_s/a$, the growth rate drops to zero. The turbulence has to generate its own vorticity through nonlinear self-sustainment [45, 46]. The turbulence is still driven by the background gradient, and
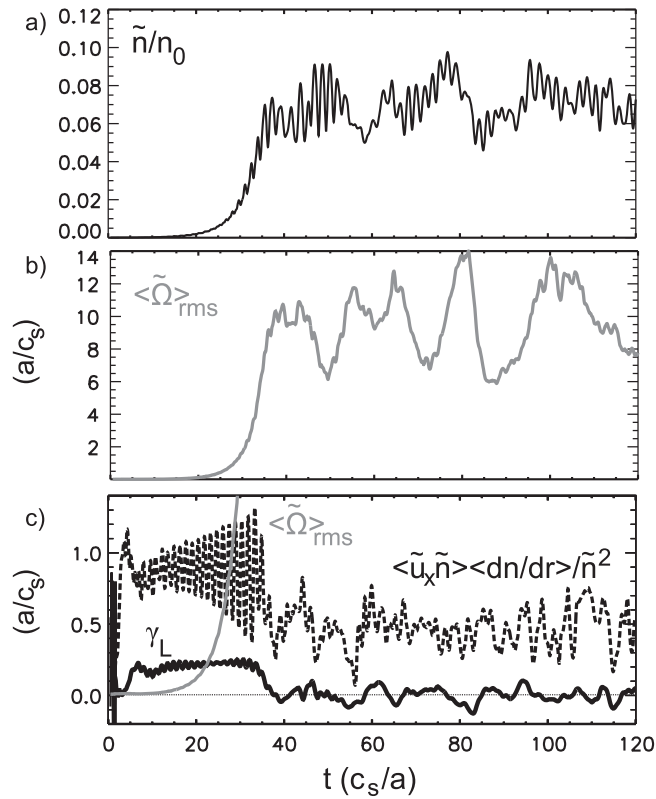
**Figure 8.** Experimental parameter case: (a) density fluctuation level, (b) vorticity fluctuation level, and (c) vorticity, growth rate $\gamma_l$, and turbulence gradient drive rate at the beginning of the simulation.



**Figure 9.** Strong turbulence case: (a) wavenumber and (b) frequency broadening shown by blue solid lines, compared to the average wavenumber and frequency shown by red dashed lines. The broadening exceeds the averaged values but is of the same order of magnitude. Data is shown in the laboratory frame of reference.

$k \neq k_l$. The total rms vorticity level $\tilde{\Omega}$ indicated by the gray shaded area in figure 6(b)) is at least similar to the linear eigenfrequency, and mostly exceeds it (black line in figure 6(b)). This seems to be sufficient to mix and disturb the drift wave during its propagation, and no typical drift wave phase velocity is measured. The results confirm that the small-scale vorticity is generated at a rate similar to the diamagnetic drift frequency [46]. The structures are only advected by the background flow. The present regime shows features of strong turbulence $\gamma_l \ll \Delta\omega$, but since the eigenfrequency is close to the frequency broadening, $\omega_l \gg \Delta\omega$ is not fulfilled. Therefore, the presented regime is closer to strong than weak turbulence.

## 5. Strong turbulence regime $\Delta\omega \gg \omega_l$

In these simulations the spectral broadening exceeds the averaged values of both frequency and wavenumber (figure 9). Since the broadening does not exceed the averaged values by orders of magnitude ($\Delta\omega / \langle\omega\rangle \approx \frac{3}{2}$, $\Delta k / \langle k\rangle \approx \frac{4}{3}$), the simulations seem to be marginally in the strong turbulence regime.

The wavenumber–frequency spectrum of density fluctuations in the drift plane at the outboard midplane is shown in figure 10. The power distribution follows more or less the mean convective velocity $\omega = u_{E \times B} k$, as indicated by the white solid line. The mean convective velocity is in the electron diamagnetic direction, which is here defined as negative. In figure 10 it appears as if the turbulence amplitude is symmetrically spread around $\omega = u_{E \times B} k$. By integrating in frequency space to estimate the mean frequency (equation (2)), a propagation in the ion diamagnetic direction in the plasma frame is observed (see figure 11(a)). This is expected for ITG modes. However, if we integrate in wavenumber space to estimate the mean wavenumber (equation (3)), and plot the frequency over this averaged wavenumber, modes at a higher wavenumber propagate in the electron diamagnetic direction in the plasma frame (figure 11(b)), which is characteristic of drift waves. Indeed, estimating the velocity by TDE using a spatial displacement of 5 mm results in the phase velocity as shown by the black dotted line in figure 11(b), which is

the effective growth rate (including nonlinear effects) is given by $\langle \tilde{u}_x \tilde{n} \rangle \langle dn/dr \rangle$ [9]. The self generated vorticity also corresponds to potential and radial velocity fluctuations $\tilde{u}_x$, which lead to transport. Furthermore, the turbulence gradient drive rate $\langle \tilde{u}_x \tilde{n} \rangle \langle dn/dr \rangle / \tilde{n}^2$ drops strongly, but not to zero. The turbulence level saturates at this point. Since the drive is still the background gradient, the vorticity is induced by adiabatic coupling, and both nonlinearities (one in the vorticity evolution and one in the density evolution) are present; thus, the turbulence is of a drift wave type. Similar to in a background shear, the nonlinear vorticity scatters small structures before they can feel a linear instability. As a consequence, linear features, such as the linear growth rate or propagation velocity, can get lost. The growth rate $\gamma_l \approx 0.2$ $c_s/a$ is much below $\langle\Omega\rangle_{rms} \approx 6$–$14$ $a/c_s$, and the vorticity rms level of the electrostatic potential fluctuations is only between 3–6 $a/c_s$. The drift wave phase velocity might survive since it is much higher than the growth rate $\omega_l \gg \gamma_l$. In figure 6(b) the black line shows the drift wave dispersion relation $\omega_l = u_{e,dia} k_y / (1 + \rho_s^2 (k_x + k_y)^2)$ (see equation (1)), which is approximated by $u_{e,dia} k / (1 + 2\rho_s^2 k^2)$ assuming isotropic structures $k_x = k_y$. The drift wave eigenfrequency (black line in figure 6(b)) is in a similar order of magnitude as the spectral broadening $\omega_l \approx \Delta\omega$ (blue line in figure 6(b)). Note that one should not only compare the eigenfrequency $\omega_l(k_l)$ at a particular scale with its spectral broadening $\Delta\omega(k_l)$, since the drift wave $\omega_l(k_l)$ is disturbed by different scales to itself
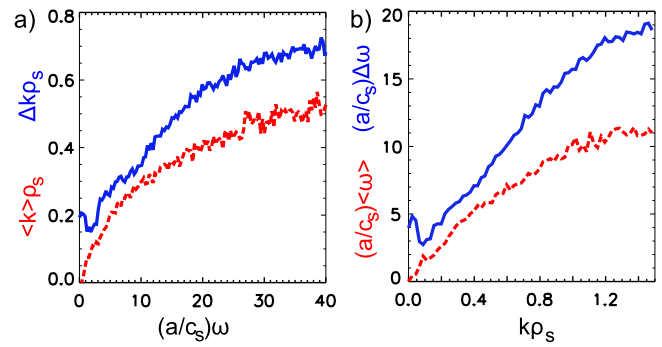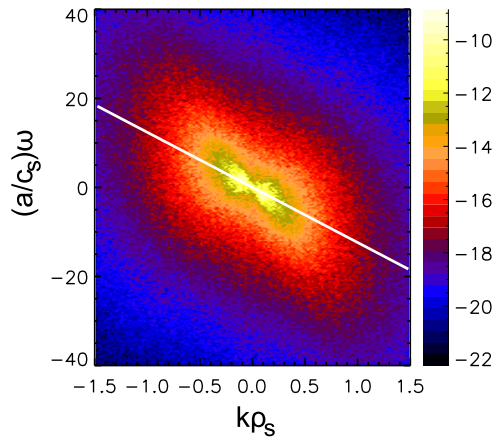
**Figure 10.** Strong turbulence case: wavenumber–frequency power spectrum $P(k, \omega)$ of density fluctuations at $\rho = 0.995$. Data is shown in the laboratory frame of reference.
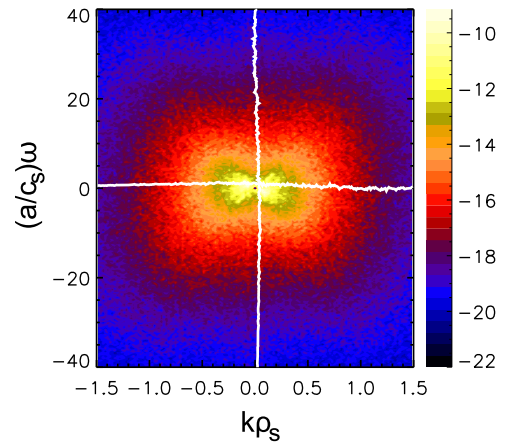


**Figure 12.** Strong turbulence case: wavenumber–frequency power spectrum $P(k, \omega)$ of density fluctuations at $\rho = 0.995$. Data is shown in the plasma frame of reference. Averaged frequencies and wavenumbers are shown by the white lines.
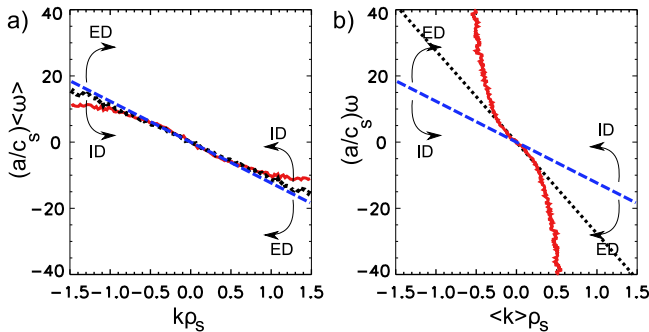


**Figure 11.** Strong turbulence case: (a) average frequency $\langle\omega\rangle$ with dependence on the wavenumber, and (b) average wavenumber $\langle k\rangle$ with dependence on the frequency $\omega$ (both red solid lines), in comparison with the mean convective velocity $\omega = u_{E\times B}k$ (blue dashed line) in the electron diamagnetic direction. Data is shown in the laboratory frame of reference. The corresponding phase velocities in the plasma frame are indicated by the arrows (ID/ED for ion/electron diamagnetic directions, respectively). The l.h.s. shows a phase velocity in ID, and the r.h.s. in ED. The velocity as measured by a DR is included by the dotted black line in (a); the velocity measured by the TDE technique is included as a black dotted line in (b).

roughly two times the background $E \times B$ velocity. Since the $E \times B$ velocity is roughly the ion diamagnetic velocity in the electron diamagnetic direction, the corresponding phase velocity as measured by TDE is the electron diamagnetic velocity as expected for electrostatic drift waves.

In summary, the structures propagate in the ion diamagnetic direction at a given wavenumber and in the electron diamagnetic direction at a given frequency. In a linear framework this seems impossible.

The reason for the discrepancy of different phase velocities $\langle\omega\rangle/k$ and $\omega/\langle k\rangle$ is the nonlinear broadening. In the case of drift wave turbulence, the power is transferred to low frequencies and low wavenumbers [47–50], leading to the power spectrum being skewed to low wavenumbers and low frequencies. This is called the inverse energy cascade [51]. At a given wavenumber $k$, the power is transferred to low

frequencies; this is responsible for a reduction in the effective frequency $\langle\omega\rangle$, and therefore also a reduction in propagation velocity $\langle\omega\rangle/k$ compared to the background velocity. As in this example, the background velocity is in the electron diamagnetic direction, which leads to a propagation in the ion diamagnetic direction in the plasma frame.

At a given frequency $\omega$, the power is transferred to lower wavenumbers. This leads to a reduction in the effective wavenumber $\langle k\rangle$ at this frequency, and therefore to an increase in the effective propagation velocity $\omega/\langle k\rangle$. As in this example, the background velocity is in the electron diamagnetic direction, and the propagation velocity in the plasma frame is also in the electron diamagnetic direction (equation (1)).

By mapping the wavenumber–frequency power spectrum $P(k, \omega)$ to the plasma frame, $P(k, \omega - u_{E\times B}k)$, it has to be considered that in the present case the background velocity is time-dependent $u_{E\times B}(t)$. Therefore, every subtime interval has to be mapped in the plasma frame, and the ensemble average is done afterward. The wavenumber–frequency power spectrum $P(k, \omega)$ in the plasma frame is shown in figure 12. It exhibits clear broadband characteristics. No signs of dispersion are observed. As in the present regime, no eigenfrequency $\omega_l = \langle\omega\rangle - u_{E\times B}k$ is detected, and $\omega_l \ll \Delta\omega$. We have seen in section 4 that the growth rate is negligible, $\gamma \ll \Delta\omega$. Therefore, the presented regime is not only marginal, but clearly in the strong turbulence regime ($\omega_l$, $\gamma_l \ll \Delta\omega$).

A shift to low frequencies due to the nonlinear energy transfer as observed by the red line in figure 11(a) is not observed by the DR [14–16] (figure 1b). By fitting a Gaussian, the skewed part at particular low frequencies of the spectrum $P(k_0, \omega)$, which results from the cascade, is basically ignored. In the average (equation (2)), the impact of this nonlinear shift is much stronger because the power is taken into account linearly and not logarithmically. The resulting Doppler shift is shown by the black dotted line in figure 11(a). The Doppler shift is more or less dispersionless, and is very close

to the mean $E \times B$ velocity; this is basically in agreement with [14–16].

## 6. Discussion and conclusion

Plasma edge turbulence is characterized by high fluctuation levels. In particular, the high level of small-scale vorticity fluctuations exhibiting strong shearing rates exceeds the growth rate by orders of magnitude $\langle \tilde{\Omega} \rangle_{\mathrm{rms}} \gg \gamma_l$ [46]; furthermore, they are of comparable levels to the eigenfrequencies of possible instabilities $\langle \tilde{\Omega} \rangle_{\mathrm{rms}} \gtrsim \omega_l$. Thereby, linear features such as growth rates and dispersion can be suppressed. This seems to be the reason behind the vanishing phase velocity in the above shown typical case for ASDEX Upgrade L-mode discharges (figure 1). These small-scale vorticity fluctuations are generated through nonlinear self-instability, and the turbulence can nonlinearly sustain itself [44–46, 49]. It is important to note that the vorticity includes contribution from electrostatic potential and ion pressure perturbations, where the later increase with the ion to electron temperature ratio can be above one in the plasma edge. If no measurements of the vorticity fluctuation level $\langle \tilde{\Omega} \rangle_{\mathrm{rms}}$ are available, it might be roughly approximated by $\langle \tilde{\Omega} \rangle_{\mathrm{rms}} \approx (1 + \tau_{\mathrm{i}})\Delta\omega$ with the ion to electron temperature ratio $\tau_{\mathrm{i}} = T_{\mathrm{i}}/T_{\mathrm{e}}$.

In the case of strong turbulence (where the frequency broadening exceeds the averaged frequency $\Delta\omega > \omega = u_{E\times B}k$) including time-varying equilibrium measurements of the phase velocity in the laboratory frame could still provide finite values even if the eigenfrequencies are suppressed by the small-scale vorticity. Broadband plasma edge turbulence shows a power law behavior in wavenumber and frequency space, which is a result of energy transfer mainly from high to low wavenumbers and frequencies. Due to the shift of energy away from the line $\omega = u_{E\times B} k$ to low wavenumbers, the wavenumber-averaged phase velocity $u(\omega) = \omega/\langle k \rangle$ will be in the direction of the background velocity. As a result of the energy transfer to low frequencies in the laboratory frame, the frequency-averaged phase velocity $u(k) = \langle \omega \rangle/k$ will be in the direction opposite that of the background velocity.

Only if the system is in the weak turbulence regime $\omega_l \gg \Delta\omega \sim \gamma_l$ can the phase velocity be used as an indicator for the underlying instability. This should be the case for core turbulence, where the fluctuation level and hence $\langle \tilde{\Omega} \rangle_{\mathrm{rms}}$ and $\Delta\omega$ are much lower. For high confinement regimes, the fluctuation levels are lower, but the difference to the L-mode is not as strong as that for the cases compared in the present study. This requires detailed investigations in the future. For example, in H-mode quasi-coherent modes with low frequency broadening are observed [52], while in I-mode a weakly coherent mode with high frequency broadening is observed [53, 54]. In general, it is recommended to verify phase velocity measurements based on a frequency-dependent technique with a wavenumber-dependent technique, and vice versa.

## ORCID iDs

P Manz ⬤ https://orcid.org/0000-0002-5724-0174
D Prisiazhniuk ⬤ https://orcid.org/0000-0002-0249-8397

## References

[1] Kadomtsev B B 1965 *Plasma Turbulence* (New York: Academic)
[2] Doerk H, Jenko F, Görler T, Told D and Pueschel M J 2012 *Phys. Plasmas* **19** 055907
[3] Navarro A B, Happel T, Görler T, Jenko F, Abiteboul J, Bustos A, Doerk H, Told D and the ASDEX Upgrade Team 2015 *Phys. Plasmas* **22** 042513
[4] Hatch D, Told D, Jenko F, Doerk H, Dunne M G, Wolfrum E, Viezzer E, Pueschel M J and the ASDEX Upgrade Team 2015 *Nucl. Fusion* **55** 063028
[5] Manz P, Boom J E, Wolfrum E, Birkenmeier G, Classen I G J, Luhmann N C Jr, Stroth U and ASDEX Upgrade Team 2014 *Plasma Phys. Control. Fusion* **56** 035010
[6] Nold B, Conway G D, Happel T, Müller H, Ramisch M, Rohde V, Stroth U and ASDEX Upgrade Team 2010 *Plasma Phys. Control. Fusion* **52** 065005
[7] Xu G S *et al* 2009 *Nucl. Fusion* **49** 092002
[8] LaBombard B, Hughes J W, Mossessian D, Greenwald M, Pipschultz B, Terry J L and the Alcator C-Mod Team 2005 *Nucl. Fusion* **45** 1658
[9] Manz P, Ribeiro T T, Scott B D, Birkenmeier G, Carralero D, Fuchert G, Müller H W, Müller S H, Stroth U and Wolfrum E 2015 *Phys. Plasmas* **22** 022308
[10] Carralero D, Birkenmeier G, Müller H W, Manz P, deMarne P, Müller S, Reimhold F, Stroth U, Wischmeier M, Wolfrum E and the ASDEX Upgrade Team 2014 *Nucl. Fusion* **54** 123005
[11] Carralero D, Manz P, Aho-Mantila L, Birkenmeier G, Brix M, Müller H W, Stroth U, Vianello N, Wolfrum E and the ASDEX Upgrade Team 2015 *Phys. Rev. Lett.* **115** 215002
[12] Manz P, Carralero D, Birkenmeier G, Müller H W, Müller S H, Fuchert G, Scott B D and Stroth U 2013 *Phys. Plasmas* **20** 102307
[13] Budaev V P, Zelenyi L M and Savin S P 2014 *J. Plasma Phys.* **81** 395810602
[14] Conway G D, Schirmer J, Klenge S, Suttrop W and Holzhauer E 2004 *Plasma Phys. Control. Fusion* **46** 951
[15] Prisiazhniuk D, Krämer-Flecken A, Conway G D, Happel T, Lebschy A, Manz P, Nikolaeva V, Stroth U and the ASDEX Upgrade Team 2016 *Plasma Phys. Control. Fusion* **59** 025013
[16] Hirsch M, Holzhauer E, Baldzuhn J, Kurzan B and Scott B D 2001 *Plasma Phys. Control. Fusion* **43** 1641
[17] Conway G D, Angioni C, Dux R, Ryter F, Peeters A G, Schirmer J, Troester C, Group C R and the ASDEX Upgrade team 2006 *Nucl. Fusion* **46** S799

[18] Happel T *et al* the ASDEX Upgrade Team 2015 *Phys. Plasmas* **22** 032503

[19] Vermare L, Hennequin P, Gürcan D, Bourdelle C, Clairet F, Garbet X, Sabot R and the Tore Supra Team 2011 *Phys. Plasmas* **18** 012306

[20] Scott B D 2002 *New J. Phys.* **4** 52

[21] Stroth U, Manz P and Ramisch M 2011 *Plasma Phys. Control. Fusion* **53** 024006

[22] Viezzer E *et al* the ASDEX Upgrade Team 2013 *Nucl. Fusion* **53** 053005

[23] Birkenmeier G *et al* the ASDEX Upgrade Team 2016 *Nucl. Fusion* **56** 086009

[24] Schmitz L, Zeng L, Rhodes T L, Hillesheim J C, Doyle E J, Groebner R J, Peebles W A, Burrell K H and Wang G 2012 *Phys. Rev. Lett.* **108** 155002

[25] Manz P *et al* 2012 *Phys. Plasmas* **19** 072311

[26] Cavedon M, Pütterich T, Viezzer E, Birkenmeier G, Happel T, Laggner F M, Manz P, Ryter F, Stroth U and ASDEX Upgrade Team 2017 *Nucl. Fusion* **57** 014002

[27] Taylor G I 1938 *Proc. R. Soc. London Ser.* A **164** 476

[28] Lin C C 1953 *Q. Appl. Maths.* **10** 295

[29] Beall J M, Kim Y C and Powers E J 1982 *J. Appl. Phys.* **53** 3933

[30] Mink F, Wolfrum E, Maraschek M, Zohm H, Horvath L, Laggner F M, Manz P, Viezzer E, Stroth U and the ASDEX Upgrade Team 2016 *Plasma Phys. Control. Fusion* **58** 125013

[31] Fedorczak N, Manz P, Thakur S C, Xu M, Tynan G R, Xu G S and Liu S C 2012 *Phys. Plasmas* **19** 122302

[32] Shao L M *et al* 2013 *Plasma Phys. Control. Fusion* **55** 105006

[33] Kobayashi T, Birkenmeier G, Wolfrum E, Laggner F M, Willensdorfer M, Stroth U, Inagaki S, Itoh S I and Itoh K 2014 *Rev. Sci. Instr.* **85** 083507

[34] Munsat T and Zweben S J 2006 *Rev. Sci. Instr.* **77** 103501

[35] Krommes J A 2002 *Phys. Rep.* **360** 1

[36] Scott B D 2006 *Contrib. Plasma Phys.* **46** 714

[37] Kendl A, Scott B D and Ribeiro T T 2010 *Phys. Plasmas* **17** 072302

[38] Cziegler I, Terry J L, Hughes J W and LaBombard B 2010 *Phys. Plasmas* **17** 056120

[39] Happel T, Blanco E and Estrada T 2010 *Re. Sci. Intrum.* **81** 10D901

[40] Nold B, Manz P, Ribeiro T T, Fuchert G, Birkenmeier G, Müller H W, Ramisch M, Scott B D and Stroth U 2014 *Phys. Plasmas* **21** 102304

[41] Sierchio J M, Cziegler I, Terry J L, White A E and Zweben S J 2016 *Rev. Sci. Intr.* **87** 023502

[42] Bulanin V V and Yafanov M V 2006 *Plasma Phys. Rep.* **32** 47

[43] Conway G D, Scott B, Schirmer J, Reich M, Kendl A and the ASDEX Upgrade Team 2005 *Plasma Phys. Control. Fusion* **47** 1165

[44] Scott B D 2005 *Phys. Plasmas* **12** 062314

[45] Scott B D 1990 *Phys. Rev. Lett.* **65** 3289

[46] Scott B D 1992 *Phys. Fluids* B **4** 2468–94

[47] Camargo S J, Biskamp D and Scott B D 1995 *Phys. Plasmas* **2** 48

[48] Manz P, Ramisch M and Stroth U 2009 *Plasma Phys. Control. Fusion* **51** 035008

[49] Manz P, Xu M, Thakur S C and Tynan G R 2011 *Plasma Phys. Control. Fusion* **53** 095001

[50] Manz P, Birkenmeier G, Ramisch M and Stroth U 2012 *Phys. Plasmas* **19** 082318

[51] Kraichnan R H 1967 *Phys. Fluids* **10** 1417

[52] Laggner F M *et al* EUROfusion MST1 Team 2016 *Plasma Phys. Control. Fusion* **58** 065005

[53] Cziegler I *et al* 2013 *Phys. Plasmas* **20** 055904

[54] Manz P *et al* 2015 *Nucl. Fusion* **55** 083004